https://doi.org/10.5194/egusphere-2025-6052
Preprint. Discussion started: 30 December 2025
© Author(s) 2025. CC BY 4.0 License.

Cross-regional NO_2 transport over the Tibetan Plateau (2005-2024): Bidirectional flux dynamics, seasonal drivers, and environmental implications

Zhenda Sun [1,2)*], Hao Yin [3)*], Zhongfeng Pan [1)], Chongyang Li [2,4)], Ke Liu [5)], Yu Yang [6)], Youwen Sun [1,4)†] and Cheng Liu [7,8,9)†]

(1 *State Key Laboratory of Opto-Electronic Information Acquisition and Protection Technology, Anhui University, Hefei, China*)

(2 *School of Environmental Science and Optoelectronic Technology, University of Science and Technology of China, Hefei 230026, China*)

(3 *School of Energy and Environment, City University of Hong Kong, Hong Kong SAR, China*)

(4 *Key Laboratory of Environmental Optics and Technology, Anhui Institute of Optics and Fine Mechanics, HFIPS, Chinese Academy of Sciences, Hefei 230031, China)*

(5 *Department of Atmospheric Measure Department of Atmospheric Measurement, Kaihang Institute of Measurement and Control Technology, Xi'an, 710065, China*)

(6 Department of Data Science, City University of Hong Kong, Hong Kong SAR, China)

(7 *Department of Precision Machinery and Precision Instrumentation, University of Science and Technology of China, Hefei 230026, China*)

(8 *Center for Excellence in Regional Atmospheric Environment, Institute of Urban Environment, Chinese Academy of Sciences, Xiamen, 361021, China*)

(9 *Key Laboratory of Precision Scientific Instrumentation of Anhui Higher Education Institutes, University of Science and Technology of China, Hefei, 230026, China*)

* *These authors contributed equally to this work*

Correspondence: Youwen Sun (ywsun@aiofm.ac.cn); Cheng Liu (chliu81@ustc.edu.cn)

Abstract:

Tropospheric NO_2 over the Tibetan Plateau (TP) reflects the combined influence of local emissions and long-range transport. We characterize the spatiotemporal variability of tropospheric NO_2 columns, surface concentrations, and transport boundary fluxes during 2005–2024 by integrating OMI and TROPOMI satellite data, ground-based observations (CNEMC), and flux diagnostics based on a closed-loop integral method. The TP shows a marked spatial gradient in tropospheric NO_2 columns, with overall levels substantially lower than those over South Asia. During the study period, NO_2 in urban areas of the plateau increased, with the most pronounced rises observed in Lhasa and Qamdo. Flux analysis shows that tropospheric NO_2 transport over the TP is quasi-symmetric across segments, manifesting as a bidirectional transport structure, with external influx dominating the southwestern segment and internal efflux toward the northeastern segment. The northeastern segment shows both a higher net flux and more rapid increases in internal efflux and external influx relative to the southwestern segment, highlighting its growing contribution to eastern China. Random forest (RF) and SHAP analyses reveal distinct dynamical controls, with winter–spring transport dominated by the upper-level westerly jet (200-400 hPa) and summer external influx primarily linked to the Indian summer monsoon (450-550 hPa). Overall, this study emphasizes the important role of the TP in cross-regional nitrogen oxide transport and provides a reference for understanding its potential impacts on regional air quality and environmental conditions.

https://doi.org/10.5194/egusphere-2025-6052
Preprint. Discussion started: 30 December 2025
© Author(s) 2025. CC BY 4.0 License.

1 Introduction

Nitrogen dioxide (NO_2) is a core component of nitrogen oxides ($NO_x = NO + NO_2$) and one of the most widely concerned atmospheric pollutants globally (Han et al., 2020; Albertin et al., 2024). As a typical photochemically active gas, NO_2 has a lifetime of only a few hours to several days, yet its reaction chains are highly efficient and complex (De Foy et al., 2015; Liu and Shi, 2021). From a health perspective, NO_2 can irritate the respiratory tract and increase the risk of asthma, cardiovascular diseases, and other conditions, and has therefore been classified by the World Health Organization as a major environmental health hazard (Erickson et al., 2020; World Health Organization, 2021, 2024). In atmospheric chemistry, NO_2 serves both as a precursor of ozone (O_3) and secondary particulate matter ($PM_{2.5}$), and as a key species in hydroxyl radical (OH) cycling, thereby profoundly influencing atmospheric oxidizing capacity and regional air quality (Atkinson, 2000; Lu et al., 2019). Its emission, transformation, and transport processes are closely linked to the active nitrogen cycle, making it an important entry point for understanding human perturbations to biogeochemical cycles. Fossil fuel combustion (vehicle exhaust, coal-fired power plants, industrial boilers), biomass burning, and certain agricultural and soil processes are the major sources of NO_2 (Barten et al., 2020; Chi et al., 2021). Meanwhile, under the influence of atmospheric transport, NO_2 and its precursors can undergo long-range regional and even transboundary transport, and by promoting ozone and secondary particulate matter formation, they indirectly affect air quality and human health in distant regions (Ma et al., 2019; Qi et al., 2023).

As the "Roof of the World," the TP has an average elevation exceeding 3,000 m, and its harsh climate and complex geographic conditions severely constrain the construction and operation of ground-based observational networks (Şerban et al., 2024; Yu et al., 2025). According to the latest deployment by the China National Environmental Monitoring Center (CNEMC, http://www.cnemc.cn/en/, last access: 4 November 2025), only a few dozen monitoring sites are currently operated in TP, Taking Tibet as an example, with six located in Lhasa and two in each of the other cities, primarily distributed across urban areas, universities, and hospitals (see Fig. 1 and Table 1). Although some research teams have locally added monitoring sites, the limited spatial coverage and site density still result in substantial constraints on systematic assessment of the atmospheric environment over the TP. Previous studies largely relied on the limited ground-based monitoring or field sampling to analyze regional pollutants (Cong et al., 2015; Nieberding et al., 2020; Cheng et al., 2021). In recent years, the development of satellite observations (such as OMI and TROPOMI) and reanalysis models has provided reliable data support for studies of the global-scale distribution and cross-regional transport of atmospheric pollutants, significantly complementing the limitations of ground observations. An increasing number of studies have used these data to analyze the spatiotemporal evolution of pollutants over the TP and surrounding regions, and, in combination with ground-based monitoring or model simulations, to further assess their cross-regional transport (Wei et al., 2022; Pan et al., 2024).

Building on these advances, NO_2 has emerged as a particularly informative diagnostic species for understanding atmospheric processes over the TP. As a reactive trace gas, its spatial patterns are shaped by the coupled influences of emissions, chemical transformation, and large-scale circulation. Consistent with the region's sparse anthropogenic activity and strong ventilation, observed NO_2 concentrations over the TP are substantially lower than those in East and South Asia. However, recent satellite and model evidence suggests that this low-NO_2 regime does not solely reflect a pristine background. Instead, it results from the combined influence of weak but

https://doi.org/10.5194/egusphere-2025-6052
Preprint. Discussion started: 30 December 2025
© Author(s) 2025. CC BY 4.0 License.

non-negligible local emissions and episodic cross-border inputs, highlighting the sensitivity of TP to both local activities and regional transport (Wang et al., 2024). Local emissions are generally limited across the TP, particularly in its western and northern sectors where populations and industrial activities are minimal. In contrast, cities such as Lhasa, Chamdo, and Shigatse exhibit discernible anthropogenic signals linked to economic development, traffic growth, winter heating, and seasonally intensified tourism (Duo et al., 2018; Jiang et al., 2023). Yet the more consequential driver of atmospheric variability is the unique position over TP at the intersection of South Asian monsoon flows and mid-latitude westerlies. These large-scale circulations can transport substantial amounts of reactive nitrogen from surrounding source regions to the high terrain, influencing the regional oxidizing environment and enhancing nitrogen deposition (Liu et al., 2015; Wang et al., 2020). Such enhanced nitrogen inputs have broader implications beyond atmospheric chemistry. They may alter the biogeochemical functioning of high-elevation ecosystems by accelerating soil acidification, disrupting nutrient stoichiometry, and shifting the carbon–nitrogen balance in alpine grasslands and wetlands that are typically nitrogen-limited (Zong et al., 2016; Chen et al., 2025). Perturbations to the oxidizing capacity of the overlying atmosphere also modulate photochemical pathways and secondary aerosol formation, with potential consequences for radiative balance and cryospheric processes such as snow albedo (Li et al., 2021; Usha et al., 2022). In parallel, growing epidemiological evidence links NO_2 exposure to adverse health outcomes, reinforcing the importance of understanding its spatial and temporal variability (Kasdagli et al., 2024; Sell et al., 2025). Collectively, these lines of evidence suggest that characterizing NO_2 over the TP is central not only to constraining regional atmospheric chemistry and transboundary transport, but also to assessing ecosystem resilience and human–environmental vulnerability in this climatically sensitive region.

Under previous studies quantifying CO transboundary fluxes using the closed-loop integration method, the TP exhibited characteristics of unidirectional accumulation accompanied by eastward transport (Sun et al., 2025). If NO_2 exhibits similar characteristics, its accumulation and potential export would extend its environmental and health impacts beyond the local scale, implying that the TP may play a more active and complex role in transboundary pollution transport than previously expected. Therefore, the study of NO_2 over the TP is not only relevant to regional air quality and ecological effects but also crucial for revealing how large-scale circulation shapes the transboundary transport patterns of pollutants. This unique geographical and dynamical setting makes it a key junction receiving emissions from South Asia and coupling with the East Asian atmospheric environment. Although NO_2 levels in eastern China are closely linked to high local emissions, transboundary inputs and redistribution over the TP may still indirectly influence regional air quality and human exposure patterns through large-scale circulation. To ensure the robustness of results and comparability across pollutants, this study continues the quantitative framework previously applied to CO fluxes, using the closed-loop integration method combined with trend regression models to estimate NO_2 transport fluxes over the TP. Based on this, we utilized OMI satellite-retrieved NO_2 products covering 2005-2024, combined with ERA5 and GEOS-CF data, to construct a long-term time series of NO_2 transport fluxes over the TP, analyzing its transboundary inputs, potential export, and the altitude-dependent effects of winds on NO_2 transport, while simultaneously emphasizing the role of circulation at different levels in shaping transport pathways over the TP.

https://doi.org/10.5194/egusphere-2025-6052
Preprint. Discussion started: 30 December 2025
© Author(s) 2025. CC BY 4.0 License.

2 Data and methods

2.1 Dataset description

The Ozone Monitoring Instrument (OMI) is a nadir-viewing spectrometer onboard NASA's Aura satellite, launched in July 2004, designed to measure backscattered solar radiation in the ultraviolet–visible spectral range (270-500 nm). The nadir spatial resolution of the observations is 13 × 24 km², with an overpass time of approximately 13:45 local time (Levelt et al., 2006). This study employs the Level-3 OMNO2d dataset (NO_2 cloud-screened total column and tropospheric column, version 3) at a resolution of 0.25° × 0.25°, covering the period from 2005 to 2024. The product groups and averages high-quality pixel-level retrievals onto fixed grids, retaining only observations with cloud fraction below 30% to ensure retrieval accuracy. Since 2007, OMI has been affected by the "row anomaly," which intensified after 2010, resulting in substantial pixel loss (Lamsal et al., 2021). To mitigate sampling bias and enhance spatiotemporal representativeness, the quality-assured retrievals were aggregated into monthly means on a 0.25° × 0.25° grid, thereby reducing random noise and ensuring the temporal continuity of the dataset.

The TROPOspheric Monitoring Instrument (TROPOMI), launched aboard the European Space Agency's Sentinel-5P satellite in October 2017, employs a push-broom imaging technique to capture sunlight scattered by the Earth's atmosphere across four spectral ranges: ultraviolet (UV), ultraviolet–visible (UV-VIS), near-infrared (NIR), and shortwave infrared (SWIR). The instrument provides near-daily global coverage with a native spatial resolution of approximately 3.5 × 5.5 km² and a local overpass time around 13:30 LT. Tropospheric NO_2 column densities are retrieved from solar backscattered radiance within the 405-465 nm interval of the UV–VIS band. In this study, the data were regridded onto a 0.25° × 0.25° grid, and only retrievals with a quality assurance (qa_value) greater than 0.75 were retained to ensure accuracy. Considering the substantial improvements in retrieval algorithms and calibration after the early operation phase, TROPOMI data from 2019 to 2024 are used.

Meteorological fields were obtained from the ERA5 global reanalysis dataset, produced by ECMWF under the Copernicus Climate Change Service (Hersbach et al., 2020). ERA5 represents a major advancement over ERA-Interim, featuring hourly temporal resolution, ~0.25° × 0.25° horizontal resolution, and full atmospheric coverage via numerous vertical levels. In this study we used the period of 2005 to 2024, selecting monthly mean data at pressure levels calculated from hourly analyses corresponding to the overpass times of the OMI satellite. Key variables selected include horizontal wind components (u, v), vertical velocity (w) and temperature (T).

NO_x emission data are derived from the EDGAR v8.1 annual inventory, which is maintained by the Joint Research Centre (JRC) of the European Commission. The database is constructed on the basis of international statistical information and national emission inventory compilation rules. Following international guidelines for greenhouse gas inventories and pollutant emission accounting methodologies, it provides a systematic integration and annual estimation of global anthropogenic emission sources (Madrazo et al., 2018; Crippa et al., 2024). As one of the most widely used anthropogenic emission inventories worldwide, EDGAR offers long-term, continuous, and comparable emission estimates for multiple atmospheric pollutants. In addition to nitrogen oxides (NO_x), its coverage also includes carbon monoxide (CO), non-methane volatile organic compounds (NMVOC), ammonia (NH_3), sulfur dioxide (SO_2), and black carbon (BC), with emission sources spanning the energy, industry, agriculture, transportation, and biomass burning sectors (Upadhyay et al., 2020). The dataset has a spatial resolution of 0.1° × 0.1°, enabling

https://doi.org/10.5194/egusphere-2025-6052
Preprint. Discussion started: 30 December 2025
© Author(s) 2025. CC BY 4.0 License.

analyses of atmospheric pollution evolution at the regional scale. In this study, annual NO_x emission data for the period 2005-2024 are selected, with a particular focus on emission changes in South Asia and the TP.

2.2 Methodology

Fig.2 presents a schematic overview of the analytical workflow, which encompasses the calculation of transport fluxes, the correction of ERA5 wind fields, and a diagnostic analysis using a Random Forest (RF) model to assess how circulation variations at different altitudes regulate NO_2 transport into the TP. Details of the RF model configuration and interpretation are provided in a dedicated section below. The closed-loop integral method for flux computation (schematically illustrated in Fig. S1), the regression model for trend analysis, and the procedures for wind-field correction and uncertainty assessment follow the framework established in our previous study on CO transport over the TP (Sun et al., 2025) and are fully documented in the Supplementary Material. Fluxes calculated over Tibet, which encompass the core areas of TP, provide representative insights for plateau-scale NO_2 transport.

2.2.1 Random Forest model

The transport processes from South Asia constitute the major external input pathway of boundary-layer NO_2 and its precursors to the TP. This cross-border transport exhibits significant differences across pressure levels, with mid-to-upper tropospheric winds potentially playing a key role in long-range transport. To further clarify the influence of *u*/*v* winds at different altitudinal layers on NO_2 transport fluxes over the TP, we employed a RF regression model, a robust non-linear ensemble learning method capable of capturing complex interactions among multilayer meteorological predictors (Breiman, 2001). RF has previously been used successfully in air quality and long-range transport studies to quantify the contributions of multiple atmospheric drivers (Kaminska, 2019; Yin et al., 2022; Wu et al., 2023). Here, the predictor variables were monthly *u*/*v* wind components from 150 to 1000 hPa (22 layers, with 50 hPa vertical resolution between 150–900 hPa and 25 hPa between 900–1000 hPa) extracted by ERA5, with zonal winds (*u*) representing the subtropical westerly jet and meridional winds (*v*) representing the South Asian monsoon. The response variable was the contemporaneous NO_2 transport flux into the southwestern TP. To ensure strict temporal and spatial consistency, all wind and flux data were aligned on a monthly basis.

The RF model consists of hundreds of independent regression trees, built using the bagging strategy that randomly resamples both samples and features to generate sub-models, while selecting the optimal splitting variable at each node. This ensemble approach effectively reduces variance and mitigates overfitting (Breiman, 2001). The dataset was randomly divided into a training set (70%) and a testing set (30%), with the former used for model fitting and the latter for independent validation on unseen data. For hyperparameter selection, we referred to existing studies and applied a systematic tuning procedure using GridSearchCV with five-fold cross-validation (Vu et al., 2019; Shi et al., 2021). The tuning parameters included the number of base learners (n_estimators), maximum tree depth (max_depth), minimum number of samples required for node splitting (min_samples_split), minimum number of samples required at leaf nodes (min_samples_leaf), and the number of features considered at each split (max_features). The final hyperparameters are listed in Table S1, with the full tuning workflow described in

https://doi.org/10.5194/egusphere-2025-6052
Preprint. Discussion started: 30 December 2025
© Author(s) 2025. CC BY 4.0 License.

Section S2.

On this basis, we employed the SHAP method to interpret the contribution of wind speed features. SHAP, grounded in the Shapley value principle from cooperative game theory, enables quantification of the marginal impact of individual features on prediction outcomes within a nonlinear model framework, and reveals the mechanisms by which different wind layers operate under varying temporal and spatial conditions (Lundberg and Lee, 2017). Unlike global feature importance metrics, SHAP values decompose each individual prediction, allowing identification of primary driving factors as well as interactions between features (Lundberg et al., 2020; Keller et al., 2021). Accordingly, SHAP provides an interpretable and quantitative basis for the dynamical regulation of cross-regional transport, enabling intuitive visualization of the enhancing or weakening effects of different wind layers on NO_2 fluxes.

2.2.2 Back-trajectories and potential source contribution function (PSCF)

Backward trajectories of near-surface air masses were simulated for seven prefecture-level cities on the TP to investigate potential source regions. To provide a representative analysis, we focused on a 5-year period (2018-2023) for trajectory simulations. Trajectories were examined for two dominant circulation regimes, the summer monsoon (June–September) and the winter westerly (December–April), traced backward for 48 hours at hourly intervals using GDAS1 (1° × 1°) meteorological data. The Potential Source Contribution Function (PSCF) was then applied to identify potential source regions contributing to high pollutant concentrations at receptor sites. For each trajectory, the residence time within each grid cell was calculated. $n_{i,j}$ denotes the total residence time of all trajectories in grid cell (i,j), while $m_{i,j}$ represents the residence time corresponding to pollutant concentrations exceeding the 75th percentile. The PSCF value is defined as:

$$PSCF_{i,j} = \frac{m_{i,j}}{n_{i,j}} \quad (1)$$

which quantifies the conditional probability that air parcels passing through grid cell (i,j) are associated with high concentrations at the receptor(Perrone et al., 2018).

To reduce uncertainty in cells with low residence times, an empirical weighting function was applied following previous work (Polissar et al., 2001; Vratolis et al., 2023). Weighting factors of 0.25, 0.5, and 0.75 were assigned to cells with total residence times below the 25th, 50th, and 75th percentiles, respectively, thereby enhancing the statistical robustness of the PSCF results.

3. Results and discussion

3.1 Variability of NO_2 flux over the TP

Based on the methodology described in Section 2, NO_2 fluxes along the TP loop region were calculated for 2005-2024 and divided into four seasons: winter (December-February), pre-monsoon (March-May), monsoon (June-September), and post-monsoon (October-November), producing corresponding gridded distributions (see Fig.3). Across all seasons, the southwestern segment consistently acts as the primary input flux region, exhibiting a spatial distribution pattern with pronounced seasonal consistency. The mean input flux per grid in the pre-monsoon, monsoon, post-monsoon, and winter seasons is 3.37, 2.97, 3.19, and 3.69 kg·s^{-1}, respectively. Input intensity is slightly enhanced during winter. During the monsoon, driven jointly by the South Asian monsoon circulation and large-scale transport systems, some grids in this region that previously

https://doi.org/10.5194/egusphere-2025-6052
Preprint. Discussion started: 30 December 2025
© Author(s) 2025. CC BY 4.0 License.

exhibited mixed fluxes shift from internal efflux to external influx, rendering the external influx belt more distinct and concentrated. In contrast, the northeastern segment displays higher seasonal stability in flux structure, with seasonal mean fluxes of –3.36, –3.28, –3.19, and –3.60 kg·s^{-1}, consistently maintaining an output state. Seasonal transitions produce minimal changes, with no pronounced abrupt shifts.

The Fig. 4 illustrates the monthly variations of NO_2 external influx and internal efflux over the TP as a whole and along its southwestern and northeastern boundaries. Overall, the cross-boundary fluxes exhibit an almost synchronous "V"-shaped cycle: they weaken month by month from spring, reach the annual minimum in July, and then gradually recover. The external influx continues to intensify in autumn, peaking in November (strongest external influx into the TP), while the internal efflux reaches its maximum in October (strongest internal efflux from the TP) and subsequently declines slightly. In terms of net flux, the TP experiences the strongest net influx in October (+0.44 kg·s^{-1}) and the strongest net efflux in September (−2.52 kg·s^{-1}).

Structurally, the southwestern boundary exhibits a consistently strong external influx throughout the year. Between June and October, the external influx increases rapidly from 3.10 kg·s^{-1} in June to the annual peak of 10.77 kg·s^{-1} in October, underscoring its persistent role as the main external influx corridor of the TP. The abrupt increase in external influx after July suggests that the evolution of monsoon circulation, adjustments in local circulation, and the influence of upper-level jets jointly drive substantial cross-boundary pollutant external influx during this period. By contrast, the internal efflux along this boundary shows smaller variations (−0.46 to −2.96 kg·s^{-1}), further confirming the external influx-dominated flux pattern. In contrast, the northeastern boundary exhibits persistently strong internal efflux year-round, with net fluxes remaining negative: it weakens to −1.72 kg·s^{-1} in July, then intensifies rapidly, reaching the annual maxima of −7.50 and −10.30 kg·s^{-1} in September and October, respectively.

Based on deseasonalized trend regressions over 2005–2024, NO_2 external influx and internal efflux along the TP loop as well as its southwestern and northeastern segments all display significant interannual increases ($p < 0.01$), with regression coefficients (R) ranging from 0.51 to 0.84, indicating that the model effectively captures long-term trends. Corresponding results are shown in Fig. 5. Spatial heterogeneity emerges in the growth rates across different boundary segments: at the northeastern boundary, influx and efflux fluxes increase at nearly the same rate (3.21 ± 0.77% yr^{-1} vs. 3.13 ± 0.45% yr^{-1}), reflecting a bidirectional transport and dynamic balance with a "channel" characteristic. This region, located in the transition zone between the TP and the central–northern China Plain, may have experienced a coupled process of regional pollution enhancement and synchronized growth in transport fluxes. By contrast, the southwestern boundary shows the slowest growth rate, with external influx remaining relatively stable (2.37 ± 0.36% yr^{-1}), indicating that the South Asian pollution external influx mechanism, after an initial phase of rapid intensification, has gradually entered a plateau stage, likely driven by multiple factors. On the one hand, NO_x emissions across South Asia have changed over the past two decades (Kurokawa and Ohara, 2020; Ding et al., 2022). These changes may partly influence the external flux entering the TP. On the other hand, monsoon-related humid meteorological conditions, such as enhanced wet scavenging, convective uplift, and boundary-layer structural changes, may have jointly contributed to more efficient NO_2 removal (Bhattarai et al., 2021; Li et al., 2024). Although both external influx and internal efflux show increasing trends, the growth rate of internal efflux along the overall loop and the southwestern boundary is slightly higher than that of external influx,

https://doi.org/10.5194/egusphere-2025-6052
Preprint. Discussion started: 30 December 2025
© Author(s) 2025. CC BY 4.0 License.

which may be driven by growing local emissions or secondary release within the TP, as reported in previous studies (Guo et al., 2022; Kong et al., 2023; Zheng et al., 2024; Zhang et al., 2025).

3.2 Potential source regions and transport pathways

The NO_2 potential source regions and the 48-hour backward-trajectory clusters for seven TP cities during the summer monsoon (June–August) and the winter westerly period (December–February) from 2018-2022 are shown in Fig. 6 and Figs. S2-S3. It reveals the pronounced differences in pollutant transport pathways and source region characteristics under these two typical circulation regimes, as well as the distinct seasonal responses of individual cities. Overall, cross-border inputs of atmospheric pollutants to the TP are primarily governed by the alternating influences of the summer monsoon and winter westerlies, with source regions and transport pathways exhibiting significant seasonal variability (Qian et al., 2011; Dong et al., 2023). PSCF results indicate that potential source regions for TP cities are mainly located in northern South Asia, while during seasonal transitions, areas controlled by the westerly belt, including Central Asia and its surroundings, also emerge as important input sources.

During the summer monsoon-dominated period, PSCF results show that cities along the southeastern margin of the TP are particularly sensitive to South Asian inputs, with high-value source regions concentrated in northern South Asia, including Nepal, northern India, and the northern Bay of Bengal. Driven by prevailing monsoon flows, pollutants are transported across the Himalayas into the southeastern TP. Cities such as Nyingchi, Shannan, and Lhasa display pronounced high-value potential source regions, directly influenced by South Asian inputs, with 23.61% of air mass trajectories arriving in Lhasa originating from these high-value South Asian regions; Nyingchi and Shannan similarly exhibit notable South Asian input signatures. Overall, pollutant inputs during the summer monsoon are characterized by shorter pathways and concentrated intensity, exerting particularly strong impacts on southeastern margin cities.

In contrast, during the winter westerly period, potential source regions shift markedly to the north and west, with high PSCF values mainly distributed over the Tarim Basin, the Central Asian industrial corridor, and the Iranian Plateau. Under the control of the westerly belt, pollutants can be transported over long distances from Central Asia and surrounding areas to the TP, forming a west-to-east input channel traversing Central Asia to the TP. These pathways are longer, more spatially diffuse, and capable of sustaining long-range transport, reflecting the well-established role of winter westerlies in distributing pollutants across continental-scale distances. Northwestern cities such as Ngari and Shigatse display high PSCF values over a broad, dispersed region, consistent with their exposure to the westerly transport system. Their source areas extend far into Central Asia, and the associated trajectories are markedly longer compared to the summer monsoon period. Conversely, southeastern cities (e.g., Nyingchi and Chamdo) show weaker wintertime connectivity to external sources, reflecting the decline of monsoonal external influx and the shielding effect of complex topography.

These contrasting seasonal signatures indicate that while monsoonal flows provide a direct and efficient conduit for South Asian pollutants into the southeastern TP, the winter westerlies expand the geographical footprint of contributing regions and enhance the potential for long-range transport into the northern and western TP (Sun et al., 2021; Kong et al., 2023; Huang et al., 2023). The unique position of TP at the interface between the monsoon and westerly systems therefore shapes a dual-source, dual-pathway transport structure, positioning the TP as a convergence and transition zone within the broader Eurasian atmospheric circulation. This distinct setting underscores the pivotal role over TP as both a receptor of cross-border pollution and a key node in the global atmospheric transport network.

3.3 Local emissions and regional transport of NO_2 over the TP

Over the past two decades (2005-2024), we divided the NO_2 column records into four consecutive five-year groups, with the corresponding changes shown in Fig. 7 and Fig. S4. Across these intervals, tropospheric NO_2 columns over South Asia and the TP have exhibited exhibited distinctly different spatiotemporal evolution patterns, which may be partly influenced by changes in emission structures and interregional transport (Fig. 8 and Fig. S5). In South Asia, NO_2 levels have been persistently elevated, with the Indo-Gangetic Plain constituting the dominant hotspot. During the mid-2000s, enhancements were largely confined to Delhi, Punjab, Haryana, and Uttar Pradesh, but subsequent phases of rapid industrialization and vehicle expansion extended the high-pollution belt across eastern provinces such as Jharkhand, Chhattisgarh, and Odisha (Kurokawa and Ohara, 2020; Ding et al., 2022). By 2015–2019, limited city-level measures such as vehicle restrictions in Delhi, temporary plant shutdowns, and the promotion of compressed natural gas proved insufficient to offset rapid urban and industrial growth, resulting in further spatial expansion of NO_2 hotspots(Choudhary et al., 2021). Only after the launch of the National Clean Air Programme in 2019 did high-value regions in the upper Indo-Gangetic Plain show signs of contraction, although industrial states in the east continued to rise, highlighting the uneven effectiveness of interventions (Ganguly et al., 2020; Gopikrishnan and Kuttippurath, 2024; Guttikunda et al., 2025).

In contrast, the TP, despite being one of cleanest regions over Asia, has experienced a steady rise in NO_2 over the same period. Since 2005, cities along the southern margin of the TP such as Lhasa, Shannan and Shigatse have experienced the most pronounced increases, with Lhasa developing a relatively stable high-concentration belt during 2015-2019. Although the growth in local emissions indeed constitutes the primary source of the NO_2 increase over the TP, the rapid rise in traffic volume, large-scale tourism activities (including the operation of numerous sightseeing buses), wintertime coal heating, and energy-intensive urban expansion have jointly elevated local NO_x emissions, especially during periods of rapid increases in vehicle ownership and construction activity (Cheng et al., 2018). The EDGAR emissions inventory corroborates this pattern, indicating that the transportation sector has become the dominant source of NO_2 emissions on the TP, exceeding contributions from the energy and industrial sectors and thereby establishing a structural basis for the long-term accumulation of NO_2. However, even after fully accounting for these local emission increases, cross-border transport from South Asia and surrounding regions still constitutes an important and persistent external driving factor.

The juxtaposition of these trends highlights a fundamental asymmetry. South Asia functions as a high-emission source region shaped by industrial cycles and uneven mitigation, whereas the TP remains a low-background but highly sensitive receptor. Temporal comparisons underscore this contrast: periods of South Asian expansion in the 2010s coincided with accelerated NO_2 growth along the southern slopes over TP. This linkage arises from the combined influence of large-scale circulation and local structural factors. Seasonal transport associated with monsoonal flow and westerlies provides sustained external inputs, which interact with emissions from heating, transport, and expanding urban activities to amplify NO_2 accumulation in key valleys and basins.

https://doi.org/10.5194/egusphere-2025-6052
Preprint. Discussion started: 30 December 2025
© Author(s) 2025. CC BY 4.0 License.

In Lhasa, for example, infrastructure expansion and rapid vehicle growth associated with China's Western Development Strategy created localized pollution hotspots that were further enhanced by transboundary external influx (Tang et al., 2022). Consequently, even modest local emissions may be magnified within a receptor environment strongly modulated by regional transport. Policy divergence further accentuates this contrast. In India, mitigation efforts remain fragmented and city-focused, producing spatially heterogeneous outcomes and enabling emissions to shift from heavily regulated cores to peripheral industrial states. By contrast, systematic framework over China under the "13th Five-Year Plan" implemented coordinated measures across energy, industry, and transport, including clean heating promotion, power sector optimization, and electric vehicle deployment (NDRC, 2016). On the TP, these measures have begun to displace coal with electricity and reduce near-surface emissions in cities such as Lhasa and Shigatse. Nevertheless, the transition remains incomplete: grid integration of hydropower and solar is limited by terrain and infrastructure constraints, and many remote settlements remain dependent on coal or biomass, preserving a fossil-fuel baseline that slows the transition toward sustained NO_2 reductions (Xing et al., 2024).

3.4 Wind layer impacts on NO_2 flux calculation

The Asian summer monsoon and the mid-latitude westerly circulation jointly control the transport of pollutants and water vapor over the TP: the former lifts near-surface pollutants to the upper troposphere through strong convection and anticyclonic circulation, enabling their dispersion into the lower stratosphere of the Northern Hemisphere, while the latter, with its persistent zonal transport capability, drives efficient external influx of pollutants from Central and East Asia into the TP and its downwind regions (Huang et al., 2023). These seasonal atmospheric circulations dominate the pollutant transport pathways around the TP and establish a critical linkage between regional air quality and global climate feedbacks. Using a random forest regression model, we analyzed the nonlinear relationships between wind speed features and NO_2 flux, enabling the model to capture the complex coupling mechanisms between wind layers and cross-regional transport. On this basis, we applied the SHAP method to quantify the contributions of wind-speed–related features, thereby evaluating the relative importance of circulation factors in predicting NO_2 cross-border transport fluxes. The corresponding SHAP results are shown in Fig. 9.

The SHAP-based attribution analysis reproduces the dual regulatory characteristics of pollutant transport over the TP: the upper-level westerly jet and the summer South Asian monsoon circulation play key regulatory roles in cross-border transport in different seasons. The model successfully captures this dual regulation, demonstrating the robustness of the interpretable framework used in this study. Furthermore, SHAP provides insights into the vertical dependency of transport pathways: the upper-tropospheric u-wind (400-150 hPa) exerts stronger cross-border transport effects during January-May and October-December, consistent with the role of the subtropical jet as a persistent cross-border transport channel; meanwhile, the mid-level v-wind (550-450 hPa) and lower-level v-wind (850-700 hPa) exhibit seasonal modulation associated with monsoon updrafts and boundary layer dynamics.

During June–September, with the establishment of the South Asian monsoon, the contribution of the upper-level westerly jet to cross-border transport exhibits pronounced seasonal variation. Previous studies have documented a northward shift of the subtropical westerly jet and

https://doi.org/10.5194/egusphere-2025-6052
Preprint. Discussion started: 30 December 2025
© Author(s) 2025. CC BY 4.0 License.

intense convective vertical transport under the South Asian monsoon (Sheng et al., 2024; Sun et al., 2021; Chen et al., 2022), which may modulate upper- and mid-level wind structures, alter the strength and stability of the westerly jet, and thereby influence both the vertical uplift from the boundary layer and the horizontal transport of pollutants across the TP. SHAP further reveals a vertically structured regulation of transport. The mid-tropospheric *v* wind exhibits seasonal control: it enhances meridional dispersion during the monsoon peak (May-November) but inhibits transport under subsidence and stable stratification conditions in winter and spring (December-April). The persistent positive contribution of the low-tropospheric vertical wind in summer and autumn highlights the role of the boundary layer monsoon circulation in coupling near-surface emissions with convective uplift, thereby promoting cross-regional diffusion of pollutants into the TP.

Interpretable machine learning enables a quantitative assessment of how cross-border transport depends on vertical wind layers, revealing the seasonal alternation in dominance among different altitude levels. By explicitly identifying the contributions of each stratified wind layer, this approach not only provides more precise constraints for pollutant transport models but also enhances our understanding of the dynamics and seasonal variability of transboundary NO_2 transport.

4 Uncertainty analysis and environmental implication

4.1 Uncertainty analysis

4.1.1 Uncertainties in satellite-derived NO_2 column retrievals

The satellite retrieval of NO_2 column concentrations is intrinsically affected by multiple sources of uncertainty, primarily including spectral fitting errors, biases in the assumed a priori vertical profile, errors in the calculation of the air mass factor (AMF), and variations in viewing geometry. Retrieval algorithms typically rely on assumed atmospheric state parameters and vertical NO_2 distributions; when these a priori conditions deviate from actual atmospheric conditions, systematic errors are introduced into the calculation of scattering weights and optical thickness. In addition, uncertainties in surface albedo and cloud parameters can alter the effective viewing geometry, forming a “coupled” error chain (Boersma et al., 2018; Van Geffen et al., 2022), which is particularly pronounced in low-loading or high-albedo regions, where small deviations in weak spectral signals can be significantly amplified.

The structural characteristics of uncertainty differ substantially among satellite products. Early OMI products were constrained by lower signal-to-noise ratios and coarser spatial resolution, with overall errors mainly governed by AMF assumptions and instrumental noise. Furthermore, the “row anomaly” and striping effects degraded both temporal continuity and spatial consistency (Boersma et al., 2018). Previous studies reported that the total uncertainty of single-pixel OMI NO_2 retrievals was approximately 35%-45%, whereas the uncertainty of TROPOMI retrievals is expected to be smaller owing to its higher signal-to-noise ratio and improved retrieval algorithms (Van Geffen et al., 2020; Verhoelst et al., 2021).

Ground-based DOAS and Pandora validation results indicate that OMI generally underestimates tropospheric NO_2 column concentrations, with biases more pronounced in mid- to high-latitude or low-loading regions, averaging around 20%-30% (Bucsela et al., 2013; Lamsal et al., 2021). In comparison, TROPOMI, benefiting from higher spectral resolution and optimized

https://doi.org/10.5194/egusphere-2025-6052
Preprint. Discussion started: 30 December 2025
© Author(s) 2025. CC BY 4.0 License.

retrieval algorithms, substantially reduces random noise, with total uncertainty expected to be lower than the 35%-45% level reported for OMI (Boersma et al., 2018; Verhoelst et al., 2021), though still constrained by systematic errors stemming from a priori profiles and atmospheric state parameters. This comparison reveals the "dual nature" of retrieval errors: while algorithmic improvements can effectively reduce random noise, structural biases cannot be fully eliminated.

In high-elevation regions such as the TP, these uncertainties are further amplified. On one hand, the extremely low NO_2 background concentrations reduce the signal-to-noise ratio in spectral fitting; on the other, complex topography and frequent cloud interference modify viewing geometry, leading to vertical sensitivity imbalance. Compared with polluted regions at mid–low latitudes, the error structure over the TP tends to be dominated by random noise rather than systematic bias. This distinction not only affects local quantitative accuracy but also increases the sensitivity of flux estimates to input uncertainties. Overall, the uncertainties in NO_2 column retrievals can be categorized into three types: (1) systematic biases, which arise from errors in a priori assumptions or atmospheric state parameters; (2) random noise, which is driven by spectral signal-to-noise ratio and meteorological disturbances; and (3) structural discontinuities, which result from variations in viewing geometry and sensor characteristics.

The identification and control of these uncertainties are essential prerequisites for ensuring the robustness and physical consistency of flux estimations. In general, recognizing and quantitatively constraining the structure of retrieval errors is critical for maintaining physical consistency and interpretability of flux trends across spatial scales. This treatment enables the study to reveal the structural features and driving mechanisms of cross-border transport under a controlled uncertainty framework.

4.1.2 Uncertainties in wind field correction

In the Closed-Loop Integral approach, the uncertainty of the wind field is one of the key factors influencing flux estimation. Because both trace gas concentrations and wind speed exhibit significant vertical gradients, their coupling effects may either amplify or attenuate the resulting flux. Directly integrating layer-by-layer wind speed can lead to weighting imbalance: upper layers with higher wind speeds but lower concentrations tend to cause overestimation, whereas lower layers with higher concentrations but smaller wind speeds may be underestimated. This "inter-layer weighting imbalance" represents one of the main sources of vertical structural error. Previous studies have indicated that uncertainty in the wind field, particularly in the vertical wind profile, is among the dominant error sources in satellite-driven flux or emission inversions. Inaccuracies in wind speed and direction, pronounced vertical gradients of wind velocity, and errors in plume or aerosol layer height can each cause the inversion results to deviate from the true values by several to tens of percent, depending on the method, region, and data quality. For instance, in mobile DOAS and point-source flux sensitivity studies, wind field uncertainty has been shown to increase flux errors by approximately 7%-50% (depending on wind-field resolution and measurement configuration). Both observational and modeling studies demonstrate that when only coarse or unrepresentative wind profiles are used, the uncertainty in flux estimates can reach several tens of percent (Wu et al., 2017; Huang et al., 2020a; Huang et al., 2020b). Moreover, satellite-based plume and fire studies have shown that interpolation and error in wind speed/direction and injection height can significantly affect lifetime and emission estimates; aerosol and AMF treatments can also introduce additional impacts on the order of 10%-25%,

https://doi.org/10.5194/egusphere-2025-6052
Preprint. Discussion started: 30 December 2025
© Author(s) 2025. CC BY 4.0 License.

suggesting that different error sources contribute comparably to the total uncertainty (Griffin et al., 2021). Based on literature synthesis and sensitivity analyses, if vertical wind structures and sampling heights are not properly treated, the uncertainty of flux estimation generally falls within the range of about 10%–30% (though it may vary by case).

To mitigate such errors, this study applies a physically constrained weighting scheme based on air-mass distribution and the vertical profile of NO_2 concentration to recalibrate the wind field, thereby constructing a more representative effective wind field. This scheme suppresses spurious contributions from high-altitude, low-density regions while enhancing the dynamical weighting of boundary-layer air masses with high concentrations, making the flux estimates more consistent with the actual transport structure. After correction, the mean wind-direction deviation is 11.09°, the average wind-speed adjustment is 1.86 m s^{-1}, and the flux uncertainty is controlled at approximately 16.35%, with detailed numerical results provided in Table S2 of the Supplement. Overall, the uncertainty of the vertical wind-field structure constitutes a non-negligible error source in closed-loop integral flux estimation, whereas the physically constrained weighted correction effectively reduces systematic bias and enhances the robustness and physical consistency of regional transport diagnostics without altering the observational constraints.

4.2 Implication

The core concern raised by the divergent NO_2 flux structures over the TP lies in their implications for human and ecological well-being. Although ground-based monitoring stations across the TP have reported declines in surface NO_2 concentrations in recent years (see Sect. S3 in the Supplement), these observations are constrained by the sparse and uneven distribution of the monitoring network. Most stations are concentrated in urban centers, while rural areas, high-altitude regions, and cross-boundary external influx corridors are almost entirely unmonitored. In contrast, satellite remote-sensing data reveal a continued increase in tropospheric NO_2 column concentrations (see Sect. S4), together with an intensifying external influx from South Asia. When assessed only from surface measurements, this mismatch between surface and column trends suggests that coupled exposure risks may be systematically underestimated. In routine monitoring practices, although official networks such as the CNEMC appear to indicate an improving situation, the total burden of reactive nitrogen in the atmospheric column over the TP continues to rise. One possible cause of this discrepancy is that the recent growth in urban NOx emissions within the TP has not been adequately captured by the limited surface monitoring network; meanwhile, relatively lenient local emission-control enforcement has further amplified this discrepancy (13th Five-Year Plan, http://www.gov.cn/zhengce/content/2017-01/05/content_5156789.htm, last access: 4 November 2025). These pollutants may intermittently mix downward, increasing near-surface exposure and altering the background oxidant levels that regulate ecosystem functions (Fig. S6). Meanwhile, the dynamic variation of the TP boundary layer further aggravates this dual risk to humans and ecosystems. In high-altitude regions, the boundary layer is relatively shallow and highly variable, usually influenced by strong diurnal cycles, winter inversions, and topographic constraints in valley cities such as Lhasa and Shigatse (Lai et al., 2023) , thereby causing disproportionate health impacts on vulnerable groups such as children, the elderly, and patients with respiratory or cardiovascular diseases. From an ecological perspective, such intermittent downward mixing can also enhance the dry and wet deposition of reactive nitrogen, leading to soil

https://doi.org/10.5194/egusphere-2025-6052
Preprint. Discussion started: 30 December 2025
© Author(s) 2025. CC BY 4.0 License.

acidification and nutrient imbalance in alpine grassland and wetland systems, which are known to be nitrogen-limited and sensitive to external inputs. Meanwhile, existing studies have shown that the continued increase in NOx emissions has been a major driver of the rapid rise in urban ozone levels across the TP in recent years (Xu et al., 2025). Although the long-range transport of ozone contributes only modestly to local ozone formation (Yin et al., 2023; Zuo et al., 2025), NO_2 transported over long distances can, to some extent, not only provide an additional precursor for tropospheric ozone over the TP but also alter the regional NOx–VOC chemical sensitivity (Ma et al., 2022; Hu et al., 2024). In the Plateau environment, this effect further enhances photochemical ozone production. The coupled influence of these processes may exacerbate the ecological risks associated with elevated ozone levels and pose health hazards to populations in high-altitude urban areas(Meng et al., 2024; Bao et al., 2024). In addition, the unique topography of the TP, including enclosed basins, steep river valleys, and urban canyon effects, further exacerbates local stagnation, such that exposure heterogeneity within a single city or basin likely exceeds the range that a limited number of monitoring instruments can capture. This, in turn, underscores the critical need to accurately assess human–ecological coupled health risks in complex high-altitude environments.

From the perspective of policy and scientific assessment, the discrepancy between surface and column signals serves as an informative signal of potential exposure risk, highlighting the necessity of establishing a multidimensional exposure assessment framework. Changes in surface concentrations can, to some extent, serve as an important indicator for evaluating the effectiveness of emission reductions, reflecting the phased improvement of near-surface urban emissions, but they cannot characterize the dynamic processes of vertical atmospheric structure and cross-boundary transport. In fact, the continuous rise of column NO_2 and the flux-driven redistribution indicate that even if surface concentrations show a downward trend, the atmospheric system still possesses the potential to accumulate and release pollutants, thereby triggering short-term high-exposure events and enhancing nitrogen deposition intensity. If the vertical redistribution process is not monitored and constrained, the true exposure levels of humans and ecosystems will be systematically underestimated, leading to delayed recognition of health and ecological risks and insufficient protection thresholds. Therefore, a flux- and exposure-oriented framework is required, integrating high-resolution satellite retrievals, vertical profile measurements, and short-term exposure and deposition models into existing monitoring networks. Such an approach can capture the "uplift–accumulation–deposition" cycles of pollutants, which are invisible to static surface averages but crucial to human and ecological health outcomes.

5. Conclusion

This study provides a comprehensive assessment of NO_2 variability and cross-border fluxes over the TP during 2005-2024, integrating multi-satellite retrievals, reanalysis-driven flux diagnostics, and machine-learning attribution. The results demonstrate that the TP, long regarded as a pristine background region, the TP is increasingly influenced by a combination of cross-boundary inputs from South Asia and local emissions. Flux analyses show persistent southwest segment external influx from South Asia and enhanced northeast segment ventilation toward East Asia; NO_2 fluxes display quasi-symmetry in each segment, manifesting as a bidirectional transport structure. Overall, these results highlight the differentiated role of reactive nitrogen in regional transport. Random Forest modeling combined with SHAP interpretation

https://doi.org/10.5194/egusphere-2025-6052
Preprint. Discussion started: 30 December 2025
© Author(s) 2025. CC BY 4.0 License.

confirms the dynamical drivers of this dual-channel structure: upper-tropospheric westerlies regulate winter–spring pathways, while summer external influx is controlled by monsoon-driven convection and anticyclonic uplift.

Despite declining surface concentrations in TP cities since 2015, tropospheric NO_2 columns have continued to rise. This divergence reflects both local emission restructuring and the strengthening influence of long-range transport. Machine-learning attribution confirms that this dynamic is sustained by the interplay of two dominant atmospheric drivers. Together, these circulations position the TP as both a receptor and a redistribution hub within the South–East Asian atmospheric system. These findings advance our understanding of the TP as more than a passive background region. This shift carries important implications for regional air quality management, as emission reductions in one region may not directly translate into improved conditions downwind or across different atmospheric layers. The TP's role in bridging continental-scale transport further underscores its importance in the global nitrogen cycle. However, in-situ observations over the TP remain limited, constraining direct validation of results derived from satellite observations and reanalysis-driven flux diagnostics. Future work will implement high-resolution ground-based measurements to better capture local NO_2 spatial heterogeneity and further evaluate cross-boundary external influx and vertical transport. Integrating ground-based observations with multi-source remote sensing is expected to improve the quantitative understanding of seasonal and local emission influences, thereby providing stronger empirical support for nitrogen cycling and air quality management across the TP.

Data availability. The OMI NO_2 dataset of this study is available for download at https://disc.gsfc.nasa.gov/ (last access: 16 June 2025). The TROPOMI NO_2 dataset of this study is available for download at https://scihub.copernicus.eu/ (last access: 16 June 2025). ERA5 monthly wind data are available download at https://cds.climate.copernicus.eu/ (last accessed: 1 June 2025). GEOS-CF dataset are available for download at https://gmao.gsfc.nasa.gov/weather_prediction/GEOS-CF/data_access/ (last accessed: 12 April 2024). The EDGAR NO_2 emission inventory is available at https://edgar.jrc.ec.europa.eu/ (last access: 31 January 2025). GEOS-Chem simulations in this study are available on request from Youwen Sun (ywsun@aiofm.ac.cn)

Author contributions. ZS prepared the manuscript and co-designed the study with HY. YS supervised and revised the manuscript. XL, ZP, CYL, YY and CL provided constructive comments.

Competing interests. The authors declare that they have no conflict of interest.

Acknowledgements. We thank the NASA Global Modeling and Assimilation Office (GMAO) for providing the GEOS-CF simulations, and the Copernicus Climate Change Service (C3S) for providing the ERA5 reanalysis data. We also express our gratitude to the GEOS-Chem team for sharing the model, and NOAA for providing the GEOS-FP meteorological files. Additionally, we thank the European Space Agency (ESA) for providing the Sentinel-5P TROPOMI CO data.

Financial support. This work is jointly supported by the National Science Fund for Excellent Young Scholars (No. 62322514), Anhui Science Fund for Distinguished Young Scholars (No.

https://doi.org/10.5194/egusphere-2025-6052
Preprint. Discussion started: 30 December 2025
© Author(s) 2025. CC BY 4.0 License.

2308085J25) and National Key Research and Development Program of China (No. 2023YFC3709502).

References

http://www.gov.cn/zhengce/content/2017-01/05/content_5156789.htm, last access: 4 November 2025.

Albertin, S., Savarino, J., Bekki, S., Barbero, A., Grilli, R., Fournier, Q., Ventrillard, I., Caillon, N., and Law, K.: Diurnal variations in oxygen and nitrogen isotopes of atmospheric nitrogen dioxide and nitrate: implications for tracing NOx oxidation pathways and emission sources, Atmos. Chem. Phys., 24, 1361-1388, 10.5194/acp-24-1361-2024, 2024.

Atkinson, R.: Atmospheric chemistry of VOCs and NOx, Atmos. Environ., 34, 2063-2101, 10.1016/s1352-2310(99)00460-4, 2000.

Bao, Y., Tian, H., and Wang, X.: Effects of climate change and ozone on vegetation phenology on the Tibetan Plateau, Sci Total Environ, 932, 172780, 10.1016/j.scitotenv.2024.172780, 2024.

Barten, J. G. M., Ganzeveld, L. N., Visser, A. J., Jiménez, R., and Krol, M. C.: Evaluation of nitrogen oxides (NOx) sources and sinks and ozone production in Colombia and surrounding areas, Atmos. Chem. Phys., 20, 9441-9458, 10.5194/acp-20-9441-2020, 2020.

Bhattarai, H., Tripathee, L., Kang, S., Sharma, C. M., Chen, P., Guo, J., and Ghimire, P. S.: Concentration, sources and wet deposition of dissolved nitrogen and organic carbon in the Northern Indo-Gangetic Plain during monsoon, J. Environ. Sci., 102, 37-52, 10.1016/j.jes.2020.09.011, 2021.

Boersma, K. F., Eskes, H. J., Richter, A., De Smedt, I., Lorente, A., Beirle, S., van Geffen, J. H. G. M., Zara, M., Peters, E., Van Roozendael, M., Wagner, T., Maasakkers, J. D., van der A, R. J., Nightingale, J., De Rudder, A., Irie, H., Pinardi, G., Lambert, J.-C., and Compernolle, S. C.: Improving algorithms and uncertainty estimates for satellite NO2 retrievals: results from the quality assurance for the essential climate variables (QA4ECV) project, Atmos. Meas. Tech., 11, 6651-6678, 10.5194/amt-11-6651-2018, 2018.

Breiman, L.: Random Forests, Machine Learning, 45, 5-32, 10.1023/a:1010933404324, 2001.

Bucsela, E. J., Krotkov, N. A., Celarier, E. A., Lamsal, L. N., Swartz, W. H., Bhartia, P. K., Boersma, K. F., Veefkind, J. P., Gleason, J. F., and Pickering, K. E.: A new stratospheric and tropospheric NO2 retrieval algorithm for nadir-viewing satellite instruments: applications to OMI, Atmos. Meas. Tech., 6, 2607-2626, 10.5194/amt-6-2607-2013, 2013.

Chen, X., Leung, L. R., Feng, Z., and Song, F.: Crucial Role of Mesoscale Convective Systems in the Vertical Mass, Water, and Energy Transports of the South Asian Summer Monsoon, J. Clim., 35, 91-108, https://doi.org/10.1175/JCLI-D-21-0124.1, 2022.

Chen, X., Shi, P., Yu, J., Hou, G., Zong, N., and Hei, H.: Nitrogen Enrichment Reshapes Contrasting Microbial Networks in Northern Tibetan Alpine Meadow vs. Steppe, Plants (Basel), 14, 10.3390/plants14172803, 2025.

Cheng, G., Zhao, S., and Huang, D.: Understanding the Effects of Improving Transportation on Pilgrim Travel Behavior: Evidence from the Lhasa, Tibet, China, Sustainability, 10, 10.3390/su10103528, 2018.

Cheng, S., Ma, J., Zheng, X., Gu, M., Donner, S., Dörner, S., Zhang, W., Du, J., Li, X., Liang, Z., Lv, J., and Wagner, T.: Retrieval of O3, NO2, BrO and OClO Columns from Ground-Based Zenith Scattered Light DOAS Measurements in Summer and Autumn over the Northern Tibetan Plateau, Remote Sens., 13, 10.3390/rs13214242, 2021.

© Author(s) 2025. CC BY 4.0 License.

Chi, Y. L., Fan, M., Zhao, C. F., Sun, L., Yang, Y. K., Yang, X. C., and Tao, J. H.: Ground-level NO concentration estimation based on OMI tropospheric NO and its spatiotemporal characteristics in typical regions of China, Atmos. Res., 264, 105821, ARTN 105821
10.1016/j.atmosres.2021.105821, 2021.

Choudhary, A., Kumar, P., Shukla, A., and Joshi, P. K.: Urban mobility associated ambient air quality and policies for environmental implications, in: Air pollution and its complications: From the regional to the global scale, Springer, 163-175, 2021.

Cong, Z., Kang, S., Kawamura, K., Liu, B., Wan, X., Wang, Z., Gao, S., and Fu, P.: Carbonaceous aerosols on the south edge of the Tibetan Plateau: concentrations, seasonality and sources, Atmos. Chem. Phys., 15, 1573-1584, 10.5194/acp-15-1573-2015, 2015.

Crippa, M., Guizzardi, D., Pagani, F., Schiavina, M., Melchiorri, M., Pisoni, E., Graziosi, F., Muntean, M., Maes, J., Dijkstra, L., Van Damme, M., Clarisse, L., and Coheur, P.: Insights into the spatial distribution of global, national, and subnational greenhouse gas emissions in the Emissions Database for Global Atmospheric Research (EDGAR v8.0), Earth Syst. Sci. Data, 16, 2811-2830, 10.5194/essd-16-2811-2024, 2024.

de Foy, B., Lu, Z., Streets, D. G., Lamsal, L. N., and Duncan, B. N.: Estimates of power plant NOx emissions and lifetimes from OMI NO2 satellite retrievals, Atmos. Environ., 116, 1-11, 10.1016/j.atmosenv.2015.05.056, 2015.

Ding, J., van der A, R., Mijling, B., de Laat, J., Eskes, H., and Boersma, K. F.: NOx emissions in India derived from OMI satellite observations, Atmos. Environ-X, 14, 10.1016/j.aeaoa.2022.100174, 2022.

Dong, X., Liu, Y., Yan, X., Wang, Y., Tan, Z., Luo, M., Li, D., Wang, Y., and Tang, S.: Compound impacts of South Asian summer monsoon and westerlies on summer precipitation over Tibetan Plateau, Clim. Dyn., 62, 3067-3087, 10.1007/s00382-023-07051-8, 2023.

Duo, B., Cui, L., Wang, Z., Li, R., Zhang, L., Fu, H., Chen, J., Zhang, H., and Qiong, A.: Observations of atmospheric pollutants at Lhasa during 2014-2015: Pollution status and the influence of meteorological factors, J Environ Sci (China), 63, 28-42, 10.1016/j.jes.2017.03.010, 2018.

Erickson, L. E., Newmark, G. L., Higgins, M. J., and Wang, Z.: Nitrogen oxides and ozone in urban air: A review of 50 plus years of progress, Environ. Prog. Sustain. Energy, 39, 10.1002/ep.13484, 2020.

Ganguly, T., Selvaraj, K. L., and Guttikunda, S. K.: National Clean Air Programme (NCAP) for Indian cities: Review and outlook of clean air action plans, Atmos. Environ-X, 8, 10.1016/j.aeaoa.2020.100096, 2020.

Gopikrishnan, G. S. and Kuttippurath, J.: Four years of National Clean Air Programme (NCAP) in Indian cities: Assessment of the impact on surface ozone during the period 2018–2022, Sust. Cities Soc., 101, 10.1016/j.scs.2024.105207, 2024.

Griffin, D., McLinden, C. A., Dammers, E., Adams, C., Stockwell, C. E., Warneke, C., Bourgeois, I., Peischl, J., Ryerson, T. B., Zarzana, K. J., Rowe, J. P., Volkamer, R., Knote, C., Kille, N., Koenig, T. K., Lee, C. F., Rollins, D., Rickly, P. S., Chen, J., Fehr, L., Bourassa, A., Degenstein, D., Hayden, K., Mihele, C., Wren, S. N., Liggio, J., Akingunola, A., and Makar, P.: Biomass burning nitrogen dioxide emissions derived from space with TROPOMI: methodology and validation, Atmos. Meas. Tech., 14, 7929-7957, 10.5194/amt-14-7929-2021, 2021.

Guo, S., Wang, Y., Zhang, T., Ma, Z., Ye, C., Lin, W., Yang Zong, D. J., and Yang Zong, B. M.: Volatile organic compounds in urban Lhasa: variations, sources, and potential risks, Front. Environ. Sci.,

https://doi.org/10.5194/egusphere-2025-6052
Preprint. Discussion started: 30 December 2025
© Author(s) 2025. CC BY 4.0 License.

10, 10.3389/fenvs.2022.941100, 2022.

Guttikunda, S. K., Dammalapati, S. K., and Pradhan, G.: Assessing air quality during India's National Clean Air Programme (NCAP): 2019–2023, Atmos. Environ., 343, 10.1016/j.atmosenv.2024.120974, 2025.

Han, K., Kim, H., and Song, C.: An Estimation of Top-Down NOx Emissions from OMI Sensor Over East Asia, Remote Sens., 12, 10.3390/rs12122004, 2020.

Hersbach, H., Bell, B., Berrisford, P., Hirahara, S., Horányi, A., Muñoz-Sabater, J., Nicolas, J., Peubey, C., Radu, R., Schepers, D., Simmons, A., Soci, C., Abdalla, S., Abellan, X., Balsamo, G., Bechtold, P., Biavati, G., Bidlot, J., Bonavita, M., De Chiara, G., Dahlgren, P., Dee, D., Diamantakis, M., Dragani, R., Flemming, J., Forbes, R., Fuentes, M., Geer, A., Haimberger, L., Healy, S., Hogan, R. J., Hólm, E., Janisková, M., Keeley, S., Laloyaux, P., Lopez, P., Lupu, C., Radnoti, G., de Rosnay, P., Rozum, I., Vamborg, F., Villaume, S., and Thépaut, J. N.: The ERA5 global reanalysis, Q. J. R. Meteorol. Soc., 146, 1999-2049, 10.1002/qj.3803, 2020.

Hu, Y., Yu, H., Kang, S., Yang, J., Chen, X., Yin, X., and Chen, P.: Modeling the transport of PM10, PM2.5, and O3 from South Asia to the Tibetan Plateau, Atmos. Res., 303, 10.1016/j.atmosres.2024.107323, 2024.

Huang, J., Zhou, X., Wu, G., Xu, X., Zhao, Q., Liu, Y., Duan, A., Xie, Y., Ma, Y., Zhao, P., Yang, S., Yang, K., Yang, H., Bian, J., Fu, Y., Ge, J., Liu, Y., Wu, Q., Yu, H., Wang, B., Bao, Q., and Qie, K.: Global Climate Impacts of Land-Surface and Atmospheric Processes Over the Tibetan Plateau, Rev. Geophys., 61, 10.1029/2022rg000771, 2023.

Huang, Y., Li, A., Xie, P., Hu, Z., Xu, J., Fang, X., Ren, H., Li, X., and Dang, B.: NOx Emission Flux Measurements with Multiple Mobile-DOAS Instruments in Beijing, Remote Sens., 12, 10.3390/rs12162527, 2020a.

Huang, Y., Li, A., Wagner, T., Wang, Y., Hu, Z., Xie, P., Xu, J., Ren, H., Remmers, J., Fang, X., and Dang, B.: The quantification of NOx and SO2 point source emission flux errors of mobile differential optical absorption spectroscopy on the basis of the Gaussian dispersion model: a simulation study, Atmos. Meas. Tech., 13, 6025-6051, 10.5194/amt-13-6025-2020, 2020b.

Jiang, K., Xing, R., Luo, Z., Li, J., Men, Y., Shen, H., Shen, G., and Tao, S.: Trends in air pollutants emissions in the Qinghai-Tibet Plateau and its surrounding areas under different socioeconomic scenarios, Sci Total Environ, 899, 165745, 10.1016/j.scitotenv.2023.165745, 2023.

Kaminska, J. A.: A random forest partition model for predicting NO(2) concentrations from traffic flow and meteorological conditions, Sci Total Environ, 651, 475-483, 10.1016/j.scitotenv.2018.09.196, 2019.

Kasdagli, M. I., Orellano, P., Perez Velasco, R., and Samoli, E.: Long-Term Exposure to Nitrogen Dioxide and Ozone and Mortality: Update of the WHO Air Quality Guidelines Systematic Review and Meta-Analysis, Int J Public Health, 69, 1607676, 10.3389/ijph.2024.1607676, 2024.

Keller, C. A., Evans, M. J., Knowland, K. E., Hasenkopf, C. A., Modekurty, S., Lucchesi, R. A., Oda, T., Franca, B. B., Mandarino, F. C., Díaz Suárez, M. V., Ryan, R. G., Fakes, L. H., and Pawson, S.: Global impact of COVID-19 restrictions on the surface concentrations of nitrogen dioxide and ozone, Atmos. Chem. Phys., 21, 3555-3592, 10.5194/acp-21-3555-2021, 2021.

Kong, H., Lin, J., Zhang, Y., Li, C., Xu, C., Shen, L., Liu, X., Yang, K., Su, H., and Xu, W.: High natural nitric oxide emissions from lakes on Tibetan Plateau under rapid warming, Nat. Geosci., 16, 474-477, 10.1038/s41561-023-01200-8, 2023.

Kurokawa, J. and Ohara, T.: Long-term historical trends in air pollutant emissions in Asia: Regional

© Author(s) 2025. CC BY 4.0 License.

Emission inventory in ASia (REAS) version 3, Atmos. Chem. Phys., 20, 12761-12793, 10.5194/acp-20-12761-2020, 2020.

Lai, Y., Chen, X., Ma, Y., Sun, F., Zhou, D., and Xie, Z.: Variation of Atmospheric Boundary Layer Height Over the Northern, Central, and Southern Parts of the Tibetan Plateau During Three Monsoon Seasons, J. Geophys. Res.-Atmos., 128, 10.1029/2022jd038000, 2023.

Lamsal, L. N., Krotkov, N. A., Vasilkov, A., Marchenko, S., Qin, W., Yang, E.-S., Fasnacht, Z., Joiner, J., Choi, S., Haffner, D., Swartz, W. H., Fisher, B., and Bucsela, E.: Ozone Monitoring Instrument (OMI) Aura nitrogen dioxide standard product version 4.0 with improved surface and cloud treatments, Atmos. Meas. Tech., 14, 455-479, 10.5194/amt-14-455-2021, 2021.

Levelt, P. F., van den Oord, G. H. J., Dobber, M. R., Malkki, A., Huib, V., Johan de, V., Stammes, P., Lundell, J. O. V., and Saari, H.: The ozone monitoring instrument, IEEE Transactions on Geoscience and Remote Sensing, 44, 1093-1101, 10.1109/tgrs.2006.872333, 2006.

Li, C., Yan, F., Kang, S., Yan, C., Hu, Z., Chen, P., Gao, S., Zhang, C., He, C., Kaspari, S., and Stubbins, A.: Carbonaceous matter in the atmosphere and glaciers of the Himalayas and the Tibetan plateau: An investigative review, Environ Int, 146, 106281, 10.1016/j.envint.2020.106281, 2021.

Li, C., Zhang, C., Kang, S., Xu, Y., Yan, F., Liu, Y., Rai, M., Zhang, H., Chen, P., Wang, P., He, C., Gao, S., and Wang, S.: Weak transport of atmospheric water-insoluble particulate carbon from South Asia to the inner Tibetan Plateau in the monsoon season, Sci. Total Environ., 922, 10.1016/j.scitotenv.2024.171321, 2024.

Liu, C. and Shi, K.: A review on methodology in O(3)-NOx-VOC sensitivity study, Environ Pollut, 291, 118249, 10.1016/j.envpol.2021.118249, 2021.

Liu, Y. W., Wang, Y. S., Pan, Y. P., and Piao, S. L.: Wet deposition of atmospheric inorganic nitrogen at five remote sites in the Tibetan Plateau, Atmos. Chem. Phys., 15, 11683-11700, 10.5194/acp-15-11683-2015, 2015.

Lu, X., Zhang, L., and Shen, L.: Meteorology and Climate Influences on Tropospheric Ozone: a Review of Natural Sources, Chemistry, and Transport Patterns, Curr. Pollut. Rep., 5, 238-260, 10.1007/s40726-019-00118-3, 2019.

Lundberg, S. M. and Lee, S.-I.: A unified approach to interpreting model predictions, Advances in neural information processing systems, 30, 2017.

Lundberg, S. M., Erion, G., Chen, H., DeGrave, A., Prutkin, J. M., Nair, B., Katz, R., Himmelfarb, J., Bansal, N., and Lee, S. I.: From Local Explanations to Global Understanding with Explainable AI for Trees, Nat Mach Intell, 2, 56-67, 10.1038/s42256-019-0138-9, 2020.

Ma, J., Zhou, X., Xu, X., Xu, X., Gromov, S., and Lelieveld, J.: Ozone and aerosols over the Tibetan Plateau, in: Asian Atmospheric Pollution, 287-302, 10.1016/b978-0-12-816693-2.00008-1, 2022.

Ma, T., Duan, F. K., He, K. B., Qin, Y., Tong, D., Geng, G. N., Liu, X. Y., Li, H., Yang, S., Ye, S. Q., Xu, B. Y., Zhang, Q., and Ma, Y. L.: Air pollution characteristics and their relationship with emissions and meteorology in the Yangtze River Delta region during 2014-2016, J. Environ. Sci., 83, 8-20, 10.1016/j.jes.2019.02.031, 2019.

Madrazo, J., Clappier, A., Belalcazar, L. C., Cuesta, O., Contreras, H., and Golay, F.: Screening differences between a local inventory and the Emissions Database for Global Atmospheric Research (EDGAR), Sci. Total Environ., 631-632, 934-941, 10.1016/j.scitotenv.2018.03.094, 2018.

Meng, X., Hua, Q., Xu, R., Shi, Y., Zhang, Y., Yan, M., Chen, W., Xu, Y., Fan, Y., Yao, Y., Wang, T., Zhang, Y., Li, H., Yu, Y., Cui, X., Chai, Q., Li, A., Sheng, M., Tang, R., Qiao, R., Li, J., Buduo,

https://doi.org/10.5194/egusphere-2025-6052
Preprint. Discussion started: 30 December 2025
© Author(s) 2025. CC BY 4.0 License.

Danzengdunzhu, Zhuoga, Hou, L., Liu, Y., Shang, J., Chen, Q., Qiu, X., Gong, J., and Zhu, T.: A prospective study on the cardiorespiratory effects of air pollution among residents of the Tibetan Plateau, Hyg. Environ. Health Adv., 12, 10.1016/j.heha.2024.100115, 2024.

NDRC: The 13th Five-year Plan for Economic and Social Development of the People's Republic of China (2016-2020), Central Compilation & Translation Press2016.

Nieberding, F., Wille, C., Fratini, G., Asmussen, M. O., Wang, Y., Ma, Y., and Sachs, T.: A long-term (2005–2019) eddy covariance data set of CO2 and H2O fluxes from the Tibetan alpine steppe, Earth Syst. Sci. Data, 12, 2705-2724, 10.5194/essd-12-2705-2020, 2020.

Pan, H., Huang, J., Li, J., Huang, Z., Wang, M., Mamtimin, A., Huo, W., Yang, F., Zhou, T., and Kumar, K. R.: The Tibetan Plateau space-based tropospheric aerosol climatology: 2007–2020, Earth Syst. Sci. Data, 16, 1185-1207, 10.5194/essd-16-1185-2024, 2024.

Perrone, M. G., Vratolis, S., Georgieva, E., Torok, S., Sega, K., Veleva, B., Osan, J., Beslic, I., Kertesz, Z., Pernigotti, D., Eleftheriadis, K., and Belis, C. A.: Sources and geographic origin of particulate matter in urban areas of the Danube macro-region: The cases of Zagreb (Croatia), Budapest (Hungary) and Sofia (Bulgaria), Sci Total Environ, 619-620, 1515-1529, 10.1016/j.scitotenv.2017.11.092, 2018.

Polissar, A. V., Hopke, P. K., and Harris, J. M.: Source regions for atmospheric aerosol measured at Barrow, Alaska, Environ Sci Technol, 35, 4214-4226, 10.1021/es0107529, 2001.

Qi, H., Duan, W., Cheng, S., Huang, Z., and Hou, X.: Spatial clustering and spillover pathways analysis of O3, NO2, and CO in eastern China during 2017–2021, Sci. Total Environ., 904, 166814, 10.1016/j.scitotenv.2023.166814, 2023.

Qian, Y., Flanner, M. G., Leung, L. R., and Wang, W.: Sensitivity studies on the impacts of Tibetan Plateau snowpack pollution on the Asian hydrological cycle and monsoon climate, Atmos. Chem. Phys., 11, 1929-1948, 10.5194/acp-11-1929-2011, 2011.

Sell, P., Plass, D., Kienzler, S., and Zeeb, H.: Environmental burden of disease resulting from long-term nitrogen dioxide exposure in Germany, BMC Public Health, 25, 79, 10.1186/s12889-024-21200-6, 2025.

Şerban, R.-D., Jin, H., Şerban, M., Bertoldi, G., Luo, D., Wang, Q., Ma, Q., He, R., Jin, X., Li, X., Tang, J., and Wang, H.: An observational network of ground surface temperature under different land-cover types on the northeastern Qinghai–Tibet Plateau, Earth Syst. Sci. Data, 16, 1425-1446, 10.5194/essd-16-1425-2024, 2024.

Sheng, C., Wu, G., Liu, Y., and He, B.: Roles of Thermal Forced and Eddy-Driven Effects in the Northward Shifting of the Subtropical Westerly Jet Under Recent Climate Change, J. Geophys. Res.-Atmos., 129, 10.1029/2023jd039937, 2024.

Shi, Z., Song, C., Liu, B., Lu, G., Xu, J., Van Vu, T., Elliott, R. J. R., Li, W., Bloss, W. J., and Harrison, R. M.: Abrupt but smaller than expected changes in surface air quality attributable to COVID-19 lockdowns, Sci Adv, 7, 10.1126/sciadv.abd6696, 2021.

Sun, Y., Yin, H., Cheng, Y., Zhang, Q., Zheng, B., Notholt, J., Lu, X., Liu, C., Tian, Y., and Liu, J.: Quantifying variability, source, and transport of CO in the urban areas over the Himalayas and Tibetan Plateau, Atmos. Chem. Phys., 21, 9201-9222, 10.5194/acp-21-9201-2021, 2021.

Sun, Z. D., Yin, H., Pan, Z., Li, C., Lu, X., Liu, K., Sun, Y., and Liu, C.: Quantifying transboundary transport flux of CO over the Tibetan Plateau: variabilities and drivers, Atmos. Chem. Phys., 25, 6823-6842, 10.5194/acp-25-6823-2025, 2025.

Tang, G., Yao, D., Kang, Y., Liu, Y., Liu, Y., Wang, Y., Bai, Z., Sun, J., Cong, Z., Xin, J., Liu, Z., Zhu,

https://doi.org/10.5194/egusphere-2025-6052
Preprint. Discussion started: 30 December 2025
© Author(s) 2025. CC BY 4.0 License.

Z., Geng, Y., Wang, L., Li, T., Li, X., Bian, J., and Wang, Y.: The urgent need to control volatile organic compound pollution over the Qinghai-Tibet Plateau, iScience, 25, 10.1016/j.isci.2022.105688, 2022.

Upadhyay, A., Dey, S., and Goyal, P.: A comparative assessment of regional representativeness of EDGAR and ECLIPSE emission inventories for air quality studies in India, Atmos. Environ., 223, 117182, ARTN 117182
10.1016/j.atmosenv.2020.117182, 2020.

Usha, K. H., Nair, V. S., and Babu, S. S.: Deciphering the Role of Aerosol-Induced Snow Albedo Feedback on Dust Emission Over the Tibetan Plateau, J. Geophys. Res.-Atmos., 127, 10.1029/2021jd036384, 2022.

van Geffen, J., Boersma, K. F., Eskes, H., Sneep, M., ter Linden, M., Zara, M., and Veefkind, J. P.: S5P TROPOMI NO2 slant column retrieval: method, stability, uncertainties and comparisons with OMI, Atmos. Meas. Tech., 13, 1315-1335, 10.5194/amt-13-1315-2020, 2020.

van Geffen, J., Eskes, H., Compernolle, S., Pinardi, G., Verhoelst, T., Lambert, J.-C., Sneep, M., ter Linden, M., Ludewig, A., Boersma, K. F., and Veefkind, J. P.: Sentinel-5P TROPOMI NO2 retrieval: impact of version v2.2 improvements and comparisons with OMI and ground-based data, Atmos. Meas. Tech., 15, 2037-2060, 10.5194/amt-15-2037-2022, 2022.

Verhoelst, T., Compernolle, S., Pinardi, G., Lambert, J.-C., Eskes, H. J., Eichmann, K.-U., Fjæraa, A. M., Granville, J., Niemeijer, S., Cede, A., Tiefengraber, M., Hendrick, F., Pazmiño, A., Bais, A., Bazureau, A., Boersma, K. F., Bognar, K., Dehn, A., Donner, S., Elokhov, A., Gebetsberger, M., Goutail, F., Grutter de la Mora, M., Gruzdev, A., Gratsea, M., Hansen, G. H., Irie, H., Jepsen, N., Kanaya, Y., Karagkiozidis, D., Kivi, R., Kreher, K., Levelt, P. F., Liu, C., Müller, M., Navarro Comas, M., Piters, A. J. M., Pommereau, J.-P., Portafaix, T., Prados-Roman, C., Puentedura, O., Querel, R., Remmers, J., Richter, A., Rimmer, J., Rivera Cárdenas, C., Saavedra de Miguel, L., Sinyakov, V. P., Stremme, W., Strong, K., Van Roozendael, M., Veefkind, J. P., Wagner, T., Wittrock, F., Yela González, M., and Zehner, C.: Ground-based validation of the Copernicus Sentinel-5P TROPOMI NO2 measurements with the NDACC ZSL-DOAS, MAX-DOAS and Pandonia global networks, Atmos. Meas. Tech., 14, 481-510, 10.5194/amt-14-481-2021, 2021.

Vratolis, S., Diapouli, E., Manousakas, M. I., Almeida, S. M., Beslic, I., Kertesz, Z., Samek, L., and Eleftheriadis, K.: A new method for the quantification of ambient particulate-matter emission fluxes, Atmos. Chem. Phys., 23, 6941-6961, 10.5194/acp-23-6941-2023, 2023.

Vu, T. V., Shi, Z., Cheng, J., Zhang, Q., He, K., Wang, S., and Harrison, R. M.: Assessing the impact of clean air action on air quality trends in Beijing using a machine learning technique, Atmos. Chem. Phys., 19, 11303-11314, 10.5194/acp-19-11303-2019, 2019.

Wang, M., Wang, Q., Ho, S. S. H., Tian, J., Zhang, Y., Lee, S.-c., and Cao, J.: Dominant influence of biomass combustion and cross-border transport on nitrogen-containing organic compound levels in the southeastern Tibetan Plateau, Atmos. Chem. Phys., 24, 11175-11189, 10.5194/acp-24-11175-2024, 2024.

Wang, W., Guan, L., Wen, Z., Ma, X., Fang, J., and Liu, X.: Atmospheric Nitrogen Deposition to a Southeast Tibetan Forest Ecosystem, Atmosphere, 11, 10.3390/atmos11121331, 2020.

Wei, J., Liu, S., Li, Z., Liu, C., Qin, K., Liu, X., Pinker, R. T., Dickerson, R. R., Lin, J., Boersma, K. F., Sun, L., Li, R., Xue, W., Cui, Y., Zhang, C., and Wang, J.: Ground-Level NO(2) Surveillance from Space Across China for High Resolution Using Interpretable Spatiotemporally Weighted Artificial Intelligence, Environ Sci Technol, 56, 9988-9998, 10.1021/acs.est.2c03834, 2022.

WHO global air quality guidelines: particulate matter (PM2.5 and PM10), ozone, nitrogen dioxide, sulfur dioxide and carbon monoxide: https://www.who.int/publications/i/item/9789240034228, last access: 4 November 2025.

Ambient (outdoor) air pollution: https://www.who.int/news-room/fact-sheets/detail/ambient-(outdoor)-air-quality-and-health, last access: 4 November 2025.

Wu, F., Li, A., Xie, P., Chen, H., Hu, Z., Zhang, Q., Liu, J., and Liu, W.: Emission Flux Measurement Error with a Mobile DOAS System and Application to NOx Flux Observations, Sensors, 17, 10.3390/s17020231, 2017.

Wu, Y., Liu, H., Liu, S., and Lou, C.: Estimate of near-surface NO(2) concentrations in Fenwei Plain, China, based on TROPOMI data and random forest model, Environ. Monit. Assess., 195, 1379, 10.1007/s10661-023-11993-1, 2023.

Xing, R., Li, Y., Luo, Z., Xiong, R., Liu, J., Jiang, K., Men, Y., Shen, H., Shen, G., and Tao, S.: Household energy use and barriers in clean transition in the Tibetan Plateau, Resour. Environ. Sustain., 18, 10.1016/j.resenv.2024.100178, 2024.

Xu, C., Lin, J., Kong, H., Jin, J., Chen, L., and Xu, X.: Rapid increases in ozone concentrations over the Tibetan Plateau caused by local and non-local factors, Atmos. Chem. Phys., 25, 9545-9560, 10.5194/acp-25-9545-2025, 2025.

Yin, H., Sun, Y. W., Notholt, J., Palm, M., Ye, C. X., and Liu, C.: Quantifying the drivers of surface ozone anomalies in the urban areas over the Qinghai-Tibet Plateau, Atmos. Chem. Phys., 22, 14401-14419, 10.5194/acp-22-14401-2022, 2022.

Yin, X., Rupakheti, D., Zhang, G., Luo, J., Kang, S., de Foy, B., Yang, J., Ji, Z., Cong, Z., Rupakheti, M., Li, P., Hu, Y., and Zhang, Q.: Surface ozone over the Tibetan Plateau controlled by stratospheric intrusion, Atmos. Chem. Phys., 23, 10137-10143, 10.5194/acp-23-10137-2023, 2023.

Yu, H., Lu, F., Hu, Z., Ma, Y., Li, M., Gu, L., Sun, F., Wang, S., Ma, W., Xie, Z., Sun, G., Huang, F., Yang, Y., Fu, C., Guo, R., Qin, Y., Wang, G., Wu, D., and Luo, H.: A Comprehensive Climate and Environment Observation Network over the central Tibetan Plateau, Bull. Amer. Meteorol. Soc., 10.1175/bams-d-24-0074.1, 2025.

Zhang, X., Ye, C., Kim, J., Lee, H., Park, J., Jung, Y., Hong, H., Fu, W., Li, X., Chen, Y., Wu, X., Li, Y., Li, J., Zhang, P., Yan, Z., Zhang, J., Liu, S., and Zhu, L.: Tropospheric NO2 Column over Tibet Plateau According to Geostationary Environment Monitoring Spectrometer: Spatial, Seasonal, and Diurnal Variations, Remote Sens., 17, 10.3390/rs17101690, 2025.

Zheng, H., Wan, X., Kang, S., Chen, P., Li, Q., Maharjan, L., and Guo, J.: Molecular characterization of organic aerosols over the Tibetan Plateau: Spatiotemporal variations, sources, and potential implications, Environ. Pollut., 340, 10.1016/j.envpol.2023.122832, 2024.

Zong, N., Shi, P., Song, M., Zhang, X., Jiang, J., and Chai, X.: Nitrogen Critical Loads for an Alpine Meadow Ecosystem on the Tibetan Plateau, Environ Manage, 57, 531-542, 10.1007/s00267-015-0626-6, 2016.

Zuo, Y., Hou, J., Chi, Y., Liu, S., and Dong, W.: Unraveling the complex drivers of ozone pollution in high-altitude urban areas: Insights from source apportionment and spatiotemporal variations, Atmos. Pollut. Res., 10.1016/j.apr.2025.102700, 2025.

Hersbach, H., Bell, B., Berrisford, P., Biavati, G., Horányi, A., Muñoz Sabater, J., Nicolas, J., Peubey, C., Radu, R., Rozum, I., Schepers, D., Simmons, A., Soci, C., Dee, D., Thépaut, J-N. (2023):

https://doi.org/10.5194/egusphere-2025-6052
Preprint. Discussion started: 30 December 2025
© Author(s) 2025. CC BY 4.0 License.

ERA5 monthly averaged data on pressure levels from 1940 to present. Copernicus Climate Change Service (C3S) Climate Data Store (CDS), DOI: 10.24381/cds.6860a573 (Accessed on 05-06-2024)

Copernicus Climate Change Service (2023): ERA5 monthly averaged data on pressure levels from 1940 to present. Copernicus Climate Change Service (C3S) Climate Data Store (CDS). DOI: 10.24381/cds.6860a573 (Accessed on 05-06-2024)

The International GEOS-Chem Community: geoschem/geos-chem: GEOS-Chem 12.2.1 (Version 12.2.1), Zenodo [code], https://doi.org/10.5281/zenodo.2580198, 2019.

Figures

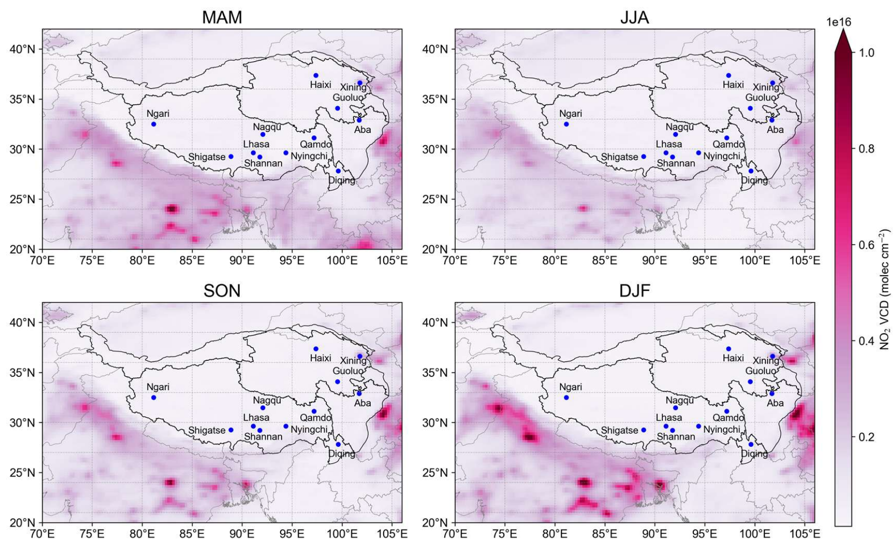

Fig. 1. Seasonal mean NO_2 VCD for the TP (2005–2024), including representative cities within the plateau and adjacent areas, derived from OMI observations.

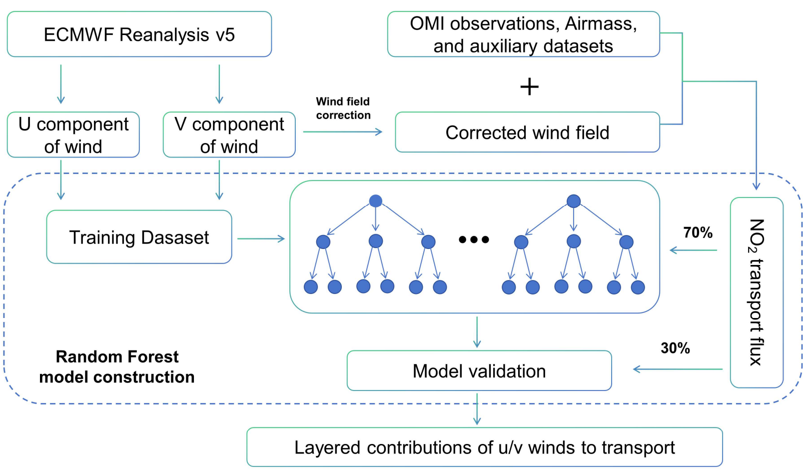

https://doi.org/10.5194/egusphere-2025-6052
Preprint. Discussion started: 30 December 2025
© Author(s) 2025. CC BY 4.0 License.

Fig. 2. Schematic framework illustrating the computation of NO_2 transport fluxes, wind-field correction, and Random Forest–based diagnostic analysis.

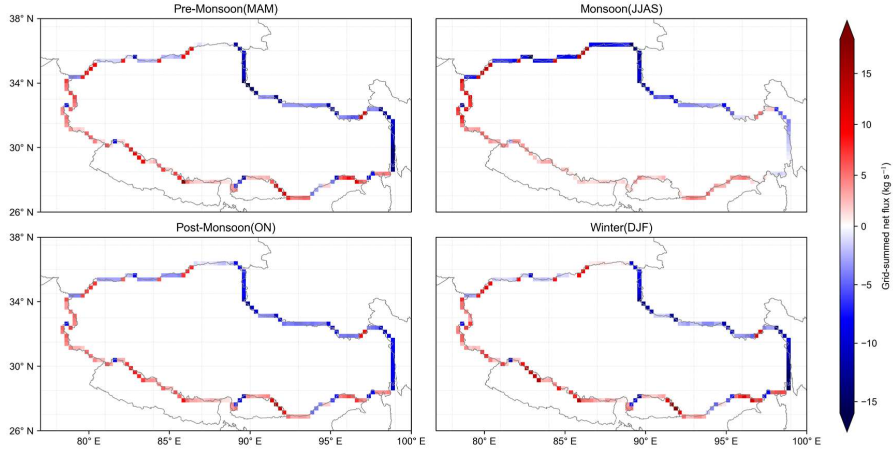

Fig. 3. Seasonal summed NO_2 fluxes for each grid cell from 2005 to 2024, divided into four periods: pre-monsoon, monsoon, post-monsoon, and winter. Red indicates external influx, while blue represents internal efflux within TP. Positive and negative values denote influx and efflux, respectively, with color intensity reflecting flux magnitude.

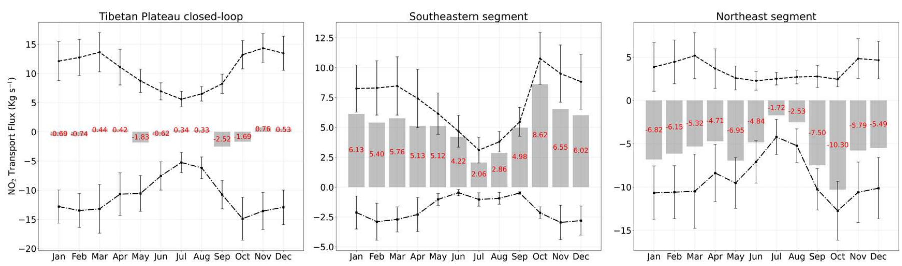

Fig. 4. Monthly NO_2 fluxes ($\pm 1\sigma$) for external influx and internal efflux across the southwestern, northeastern, and enclosed boundary segments of the TP during 2005-2024. Gray bars indicate the net flux, with red numbers denoting the net flux values.

https://doi.org/10.5194/egusphere-2025-6052
Preprint. Discussion started: 30 December 2025
© Author(s) 2025. CC BY 4.0 License.

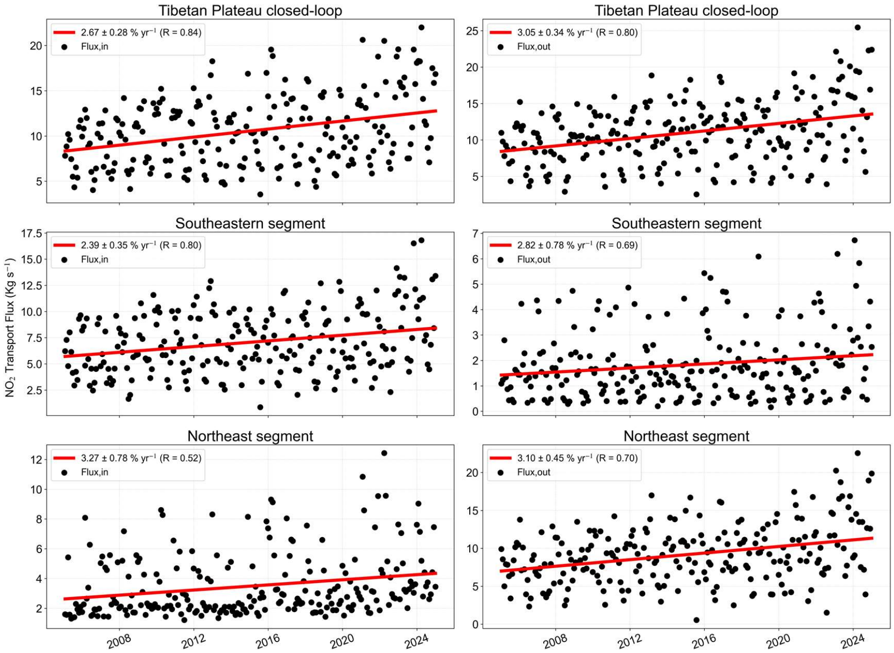

Fig. 5. Interannual evolution of NO_2 influxes and effluxes across the closed-loop, southwestern, and northeastern boundaries of the plateau (2005-2024), based on biweekly means. Black points represent NO_2 fluxes, and the red line denotes the long-term trend fitted using a trend model.

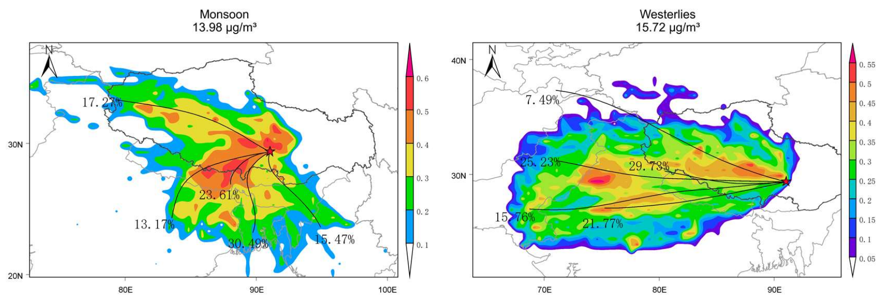

Fig. 6. PSCF-derived potential source regions and clustered back trajectories for Lhasa, categorized into the monsoon and westerly periods.

https://doi.org/10.5194/egusphere-2025-6052
Preprint. Discussion started: 30 December 2025
© Author(s) 2025. CC BY 4.0 License.

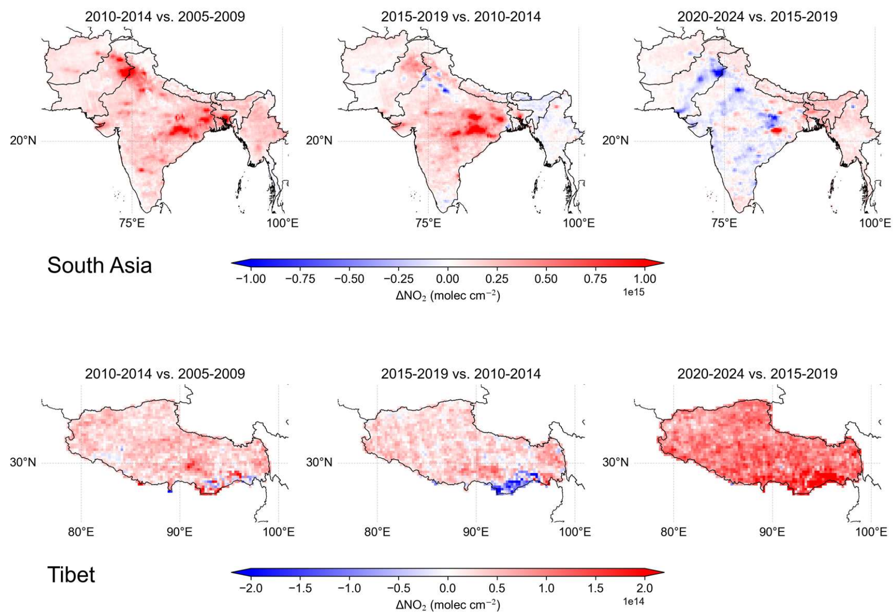

Fig. 7. Five-year grouped changes in NO_2 column concentrations over South Asia and the TP from 2005 to 2024.

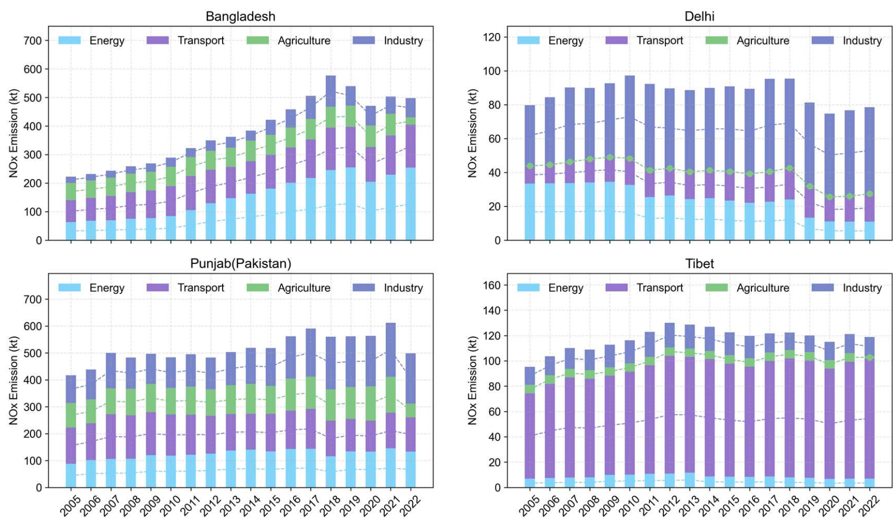

Fig. 8. Annual NO_x emissions by sector (energy, transport, agriculture, and industry) across Bangladesh, Delhi, Punjab (Pakistan), and Tibet, derived from EDGAR and aggregated over all pixels within administrative boundaries.

https://doi.org/10.5194/egusphere-2025-6052
Preprint. Discussion started: 30 December 2025
© Author(s) 2025. CC BY 4.0 License.

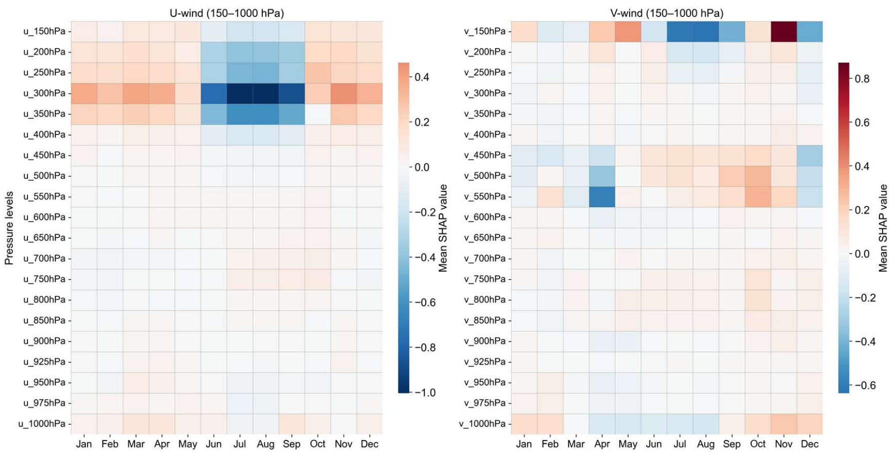

Fig. 9. SHAP-based contributions of U- and V-wind (150-1000 hPa) to NO_2 transport flux variations across the southwestern TP boundary, with red and blue indicating positive and negative contributions, respectively.

Tables

Table 1. Geographical, demographic, and monitoring site information for major cities on the Tibetan Plateau. Population statistics are based on the 2020 nationwide population census issued by the National Bureau of Statistics of China.

City	Number of Monitoring Sites	Latitude (°N)	Longitude (°E)	Avg. Altitude (km)	Population ($\times 10^5$)	Area (km^2)	Population Density ($persons/km^2$)
Ngari	2	32.5	80.1	4.5	12	345,000	3.48
Shigatse	2	29.3	88.9	4	80	182,000	43.96
Lhasa	6	29.7	91.1	3.7	87	31,700	274.45
Shannan	2	29.2	91.8	3.7	35	79,300	44.14
Nagqu	2	31.5	92.1	4.5	50	430,000	11.63
Nyingchi	2	29.6	94.4	3.1	23	117,000	19.66
Qamdo	3	31.1	97.2	3.4	76	110,000	69.09
Diqing	2	27.8	99.7	3.5	39	23,900	163.18
Haixi	1	37.4	97.4	4.8	47	325,800	14.43
Guoluo	1	34.5	100.3	4.3	21	76,400	27.49
Xining	4	36.6	101.7	2.3	247	7,700	3207.79
Aba	3	32.9	101.7	3.8	82	84,200	97.39